

Network modelling of yield-stress fluid flow in randomly disordered porous media

Cláudio P. Fonte,¹ Elliott Sutton,^{1,2} Kohei Ohie,³ Eleanor Doman,⁴ Yuji Tasaka,³ and Anne Juel^{2,5}

¹*Department of Chemical Engineering, The University of Manchester, Oxford Road, Manchester M13 9PL,*

UK

²*Manchester Centre for Nonlinear Dynamics, The University of Manchester, Oxford Road, Manchester M13 9PL,*

UK

³*Laboratory for Flow Control, Division of Mechanical and Aerospace Engineering, Faculty of Engineering, Hokkaido University, Sapporo N13W8, Hokkaido 060-8628, Japan*

⁴*Department of Mathematics, The University of Manchester, Oxford Road, Manchester M13 9PL,*

UK

⁵*Department of Physics and Astronomy, The University of Manchester, Oxford Road, Manchester M13 9PL,*

UK

(*Electronic mail: anne.juel@manchester.ac.uk)

(Dated: 11 March 2026)

Yield-stress fluid flow through porous media is governed by a strong coupling between rheology and pore-scale geometry, leading to nonlinear, non-Darcy transport and pronounced channelisation near yielding. We develop a pore-network model for Herschel-Bulkley flow in two-dimensional disordered porous media, including optional wall slip. The network is closed by a physics-based pressure-flow relation for a converging-diverging throat, so that yielding and post-yield transport emerge directly from the pore-scale fluid mechanics without fitted resistance parameters. Benchmarking against direct numerical simulations shows that the model captures both the bulk pressure drop and the evolution of the flow topology from spatially distributed transport to strongly channelised flow. The framework also captures the leading effect of wall slip, which lowers the pressure gradient required for transport and reactivates pathways that remain blocked in the no-slip case. Using the model across different porous geometries, we show that near-yield pressure losses are governed by constriction statistics rather than by an obstacle-scale length. In particular, rescaling with the domain-averaged minimum throat width collapses the plastic-dominated response across porosities, identifying the dissipation-relevant geometric scale for viscoplastic transport in this regime.

The flow of yield-stress fluids through porous media is central to applications including enhanced oil recovery^{1,2}, filtration^{3,4}, coating penetration^{5,6}, and soil remediation⁷⁻⁹. In these systems, non-Darcy behaviour is intrinsic: flow begins only above a finite pressure threshold, the relation between flow rate and pressure drop is nonlinear, and transport near yielding becomes highly heterogeneous because only part of the pore space is mobilized¹⁰⁻¹². Wall slip, commonly observed in soft glassy and particulate materials, can add further complexity to this behaviour by reducing wall friction, lowering the apparent yield threshold, and suppressing channelisation when slip is sufficiently strong^{11,13-16}. Predicting how yielding, pore-scale disorder, and slip combine to determine the macroscopic flow response remains a major challenge.

Direct numerical flow simulations can resolve these effects, but their cost and numerical complexity limit their use in large or strongly disordered porous domains. Pore-network models offer an efficient reduced-order description by representing the void space as pores connected by throats governed by local pressure-flow relations^{17,18}. Their predictive power therefore depends critically on the fidelity of the throat-scale closure. This is especially true near the yielding transition, where the global response is controlled by a small subset of constrictions and even modest local modelling errors can lead to large errors in the predicted threshold and post-yield transport. Existing network models for viscoplastic flow capture some qualitative trends^{4,19}, but discrepancies remain pronounced close to yielding²⁰⁻²², and some formulations rely on fitted resistance

parameters^{23,24}. A predictive network model that incorporates both yield-stress rheology and wall slip without empirical calibration is, to the best of our knowledge, still lacking in the literature.

In this Letter, we develop a pore-network model for Herschel-Bulkley flow in two-dimensional disordered porous media. The network is closed by a physics-based pressure-flow relation for a converging-diverging throat, with optional wall slip, so that both yielding and post-yield transport emerge directly from the pore-scale fluid mechanics without fitted resistance parameters. Comparison against direct numerical simulations shows that the model captures the macroscopic departure from Darcy behaviour through the yielding transition. The framework further reveals that near-yield pressure losses are controlled by constriction statistics rather than by an obstacle-scale length: rescaling with the domain-averaged minimum throat width collapses the plastic-dominated response across porosities, identifying the dissipation-relevant geometric scale in this regime.

TABLE I. Geometric characteristics of the porous media considered. Case CT is identical to that studied by Chaparian and Tammissola¹¹.

Case	L/R	ϕ	\bar{h}_{\min}/R
CT	50	0.7	0.795
G1	20	0.600	0.564
G2	20	0.702	0.830
G3	20	0.804	1.23

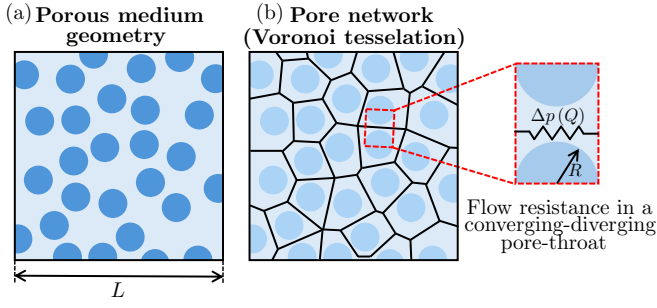


FIG. 1. (a) Two-dimensional porous medium formed by randomly placed circular obstacles. (b) Voronoi-based pore network: vertices are pores and edges are throats, with resistance set by the converging–diverging gap between neighbouring obstacles.

We start by considering two-dimensional porous domains of size $L \times L$ formed by the void space between randomly placed, non-overlapping circular obstacles of radius R [see Fig. 1(a)]. Table I lists the distinct realisations considered in this study, spanning a range of morphologies and porosities. In addition to the obstacle radius, R , and domain size, L , each porous medium is characterised by its porosity, $\phi = 1 - \pi R^2 N / L^2$, where N denotes the total number of obstacles in the domain. This work also introduces the mean minimum pore-throat width, \bar{h}_{\min} , as a relevant statistical descriptor of the porous medium.

To construct a pore-network representation, we compute the Voronoi tessellation of the obstacle centroids [see Fig. 1(b)]. The Voronoi vertices define pores and the Voronoi edges define throats, yielding a graph $(\mathcal{V}, \mathcal{E})$ with set of pores \mathcal{V} and set of throats \mathcal{E} . Flow is modelled by mass conservation at each pore and a throat pressure-flow law on each edge. For pore $i \in \mathcal{V}$,

$$\sum_j Q_{i \rightarrow j} = 0, \quad (1)$$

where the sum is over all neighbours j connected to i by $(i, j) \in \mathcal{E}$. Each edge is assigned a fixed orientation $i \rightarrow j$, and $Q_{i \rightarrow j}$ is taken positive in that direction. The pressure drop across a throat satisfies

$$p_i - p_j = \mathcal{P}(Q_{i \rightarrow j}), \quad (2)$$

$$Q = \begin{cases} \frac{2h\alpha(Gh - \tau_s)^\beta}{\sqrt{1+h^2}} + \frac{2nK}{G^2} \left(\frac{Gh - \tau_0}{K} \right)^{\frac{n+1}{n}} \frac{(n+1)Gh + n\tau_0}{(n+1)(2n+1)} + \varepsilon(G), & Gh > \tau_0, \\ \frac{2h\alpha(Gh - \tau_s)^\beta}{\sqrt{1+h^2}} + \varepsilon(G), & \tau_s < Gh \leq \tau_0, \\ \varepsilon(G), & Gh \leq \tau_s. \end{cases} \quad (6)$$

where $\varepsilon(G) = \frac{2}{3} Gh^3 / \mu_{\text{reg}}$ is a regularisation parameter corresponding to the volumetric flow rate of a Newtonian fluid with viscosity μ_{reg} , introduced in (6) to improve numerical robust-

ness. We choose μ_{reg} sufficiently large that $\varepsilon(G)$ is negligible compared with the physical contributions in the yielded regimes, while preventing exactly zero flow.

where $\mathcal{P}(\cdot)$ is the (generally nonlinear) pressure-flow relation associated with the converging-diverging gap between neighbouring obstacles. Although network channels are represented as straight Voronoi edges, the converging-diverging throat shape set by the interstitial gap between two neighbouring circular obstacles is embedded in the closure $\mathcal{P}(Q_{i \rightarrow j})$. We estimate the throat-scale pressure drop by modelling steady, unidirectional flow of a generalised Newtonian fluid through the gap. Introducing local coordinates with x along the Voronoi edge and y transverse, the domain is $x \in [0, 2R]$ and $y \in [-h(x), h(x)]$, with $h(x) = h_{\min} + R - \sqrt{R^2 - (x-R)^2}$, where $2h_{\min}$ is the minimum pillar separation.

Under the one-dimensional flow approximation, $\partial p / \partial y = 0$, the streamwise momentum balance reduces to

$$-\frac{\partial}{\partial y} \left(\eta(\dot{\gamma}) \frac{\partial u}{\partial y} \right) = G(x), \quad G(x) = -\frac{dp}{dx}, \quad (3)$$

where $u(x, y)$ is the streamwise velocity and $\dot{\gamma} = |\partial u / \partial y|$. We use the Herschel-Bulkley law $\eta(\dot{\gamma}) = \tau_0 / \dot{\gamma} + K \dot{\gamma}^{n-1}$ to describe viscoplasticity, with yield stress τ_0 and consistency and power-law indices K and n . At the walls we impose a slip condition, $u(x, \pm h) = u_s(x)$, with

$$u_s(x) = \frac{\alpha(\tau_w(x) - \tau_s)^\beta}{\sqrt{1+h'(x)^2}}, \quad \tau_w(x) = G(x)h(x), \quad (4)$$

where α is the slip coefficient, β a slip exponent (taken as $\beta = 1$ in this work²⁵), and τ_s a slip yield stress. The factor $1/\sqrt{1+h'(x)^2}$ accounts for wall inclination by projecting tangential slip onto the streamwise direction.

The flow rate is related to the local pressure gradient in the pore throat by

$$Q = \int_{-h(x)}^{h(x)} u(x, y) dy. \quad (5)$$

Solving (3) subject to (4) yields the local relation between Q and $G(x)$,

Finally, the pressure-drop functional entering (2) is obtained by integrating the local pressure gradient along the pore throat at fixed flow rate. By symmetry under flow reversal, it is odd, and we write

$$\mathcal{P}(Q) = \text{sgn}(Q) \int_0^{2R} G(x; |Q|) dx. \quad (7)$$

Since $G(x; |Q|)$ cannot be obtained in closed form, we compute it by numerically inverting (6) for each x , and evaluate (7) using numerical quadrature.

For a network with N_v interior pores and N_e throats, enforcing mass conservation (1) together with the throat pressure-flow relation (2) yields a coupled system of $N_v + N_e$ nonlinear equations, written compactly as $\mathbf{F}(\mathbf{z}) = \mathbf{0}$. Here \mathbf{z} collects the throat flow rates together with the pressures at interior pores; inlet/outlet pore pressures are prescribed and excluded from the vector of unknowns. We write $\mathbf{F} = [\mathbf{f}(\mathbf{Q}), \mathbf{g}(\mathbf{p}, \mathbf{Q})]^\top$, where the N_v mass-balance residuals are

$$f_i = \sum_j Q_{i \rightarrow j}, \quad i \in \mathcal{V}, \quad (8)$$

and the N_e throat residuals enforce the pressure-flow relation,

$$g_{ij} = p_i - p_j - \mathcal{P}(Q_{i \rightarrow j}), \quad (i, j) \in \mathcal{E}. \quad (9)$$

We solve $\mathbf{F}(\mathbf{z}) = \mathbf{0}$ using a Newton-type method with trust-region globalisation, implemented in Julia via `NonlinearSolve.jl`; the Jacobian is formed by central finite differences. Because the system becomes stiff near yielding, we use continuation in the imposed inlet pressure: solutions are computed along a sweep of p_{in} , using the previous converged solution (with linear extrapolation from the last two steps) as the initial guess. Convergence is declared when the residual norm satisfies prescribed absolute and relative tolerances. The Julia implementation used in this study is openly available on GitHub²⁶.

Network-model predictions are benchmarked against two sets of fully resolved two-dimensional simulations: the viscoplastic simulations of Chaparian and Tammissola¹¹, which employ an augmented-Lagrangian finite-element formulation to accurately resolve yielded and unyielded regions, and our own direct simulations in the Newtonian limit. Full details of the numerical methodology for the Newtonian-limit simulations, including the discretisation and solver settings, are similar to those reported by Sutton *et al.*²⁷; only the numerical results are presented here.

For consistency, we adopt the non-dimensionalisation of Chaparian and Tammissola¹¹, based on the obstacle radius R , and denote the bulk Bingham number and streamwise pressure gradient by $(\mathcal{B}, \mathcal{G})$. Thus,

$$\mathcal{G} = \frac{\Delta p}{L} \frac{R}{K(\bar{U}/R)^n}, \quad \mathcal{B} = \frac{\tau_0}{K(\bar{U}/R)^n}, \quad (10)$$

where Δp is the imposed pressure drop across the porous domain and $\bar{U} = Q_T/L$ is the mean inlet velocity, with Q_T the total flow rate percolating through the network. Unlike Chaparian and Tammissola¹¹, however, we define the mean velocity using the full domain width L rather than the open inlet

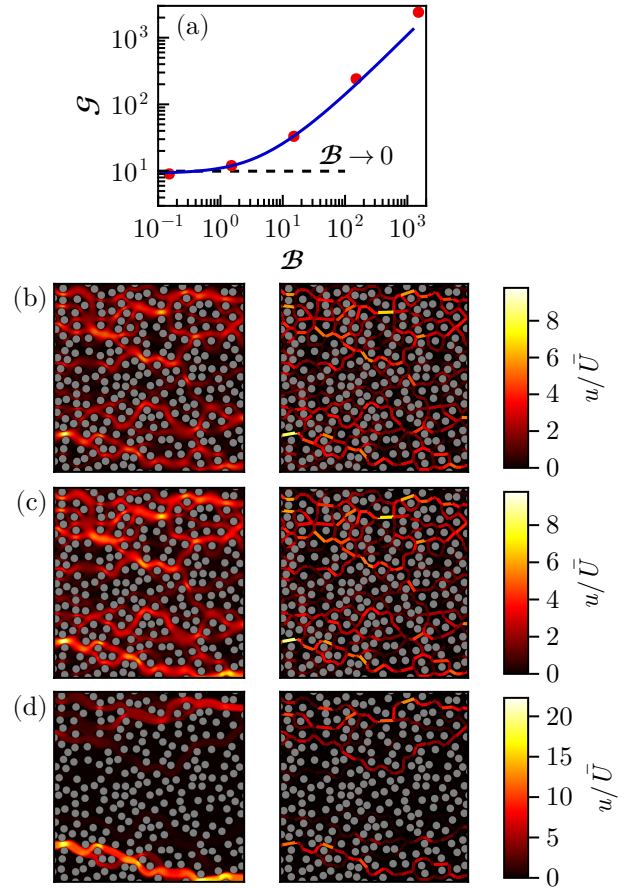


FIG. 2. (a) No-slip response in geometry CT: dimensionless bulk pressure gradient \mathcal{G} versus bulk Bingham number \mathcal{B} . Solid line, present network model; markers, direct numerical simulations of Chaparian and Tammissola¹¹. The horizontal dashed line denotes the Newtonian limit ($\mathcal{B} \rightarrow 0$) from the fully resolved flow simulations. (b-d) Velocity magnitude maps in geometry CT without slip, comparing direct numerical simulations (left) and the network model (right) for (b) $\mathcal{B} = 0$, (c) $\mathcal{B} = 1.5$, and (d) $\mathcal{B} = 150$. The left-hand panels in (c) and (d) are reproduced from Chaparian and Tammissola¹¹ under CC BY 4.0.

length L_{inl} . Their reported values of \mathcal{B} and \mathcal{G} were therefore rescaled by $(L/L_{\text{inl}})^n$ to match the present definition; for the Bingham-fluid data considered here, this reduces to L/L_{inl} .

Fig. 2(a) compares the predicted no-slip response in geometry CT (cf. Table I) with the numerical results. The network model reproduces the monotonic increase of \mathcal{G} with \mathcal{B} , recovering the Newtonian limit as $\mathcal{B} \rightarrow 0$ and the linear viscoplastic scaling $\mathcal{G} = c\mathcal{B}$ at large \mathcal{B} , where c depends on the geometry. This large- \mathcal{B} regime reflects the fact that only a small number of flow pathways remain fluidised [cf. Fig. 2(d)].

Fig. 2(b-d) compare velocity magnitude maps over a range of \mathcal{B} . At small \mathcal{B} , the network model reproduces both the spatially widespread flow topology, with most pathways remaining active, and the distribution of local velocities. With increasing \mathcal{B} , it captures the onset of channelisation and the progressive shutdown of secondary pathways. Even close

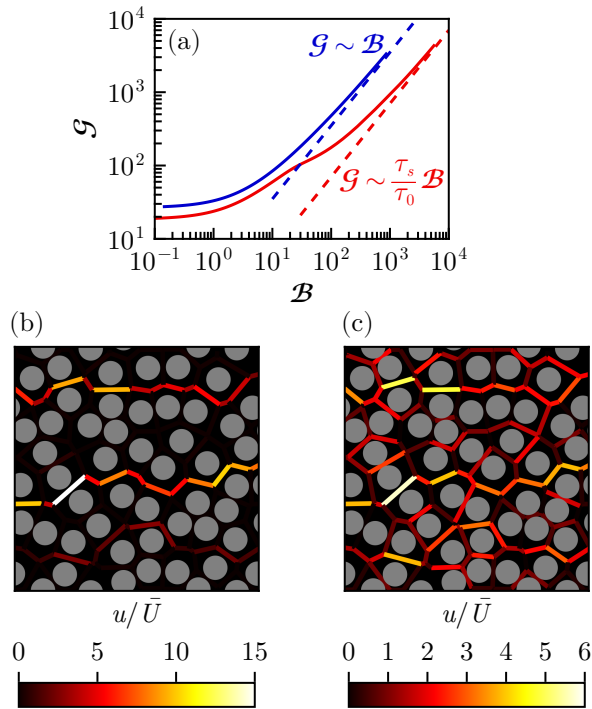


FIG. 3. Effect of wall slip on the bulk response and flow topology in geometry G1. (a) Dimensionless bulk pressure gradient \mathcal{G} as a function of bulk Bingham number \mathcal{B} for the no-slip case and for a slipping wall with $\alpha = 0.1R/K$ and $\tau_s = 0.2\tau_0$. The dashed lines indicate the large- \mathcal{B} asymptotic scalings, $\mathcal{G} \sim \mathcal{B}$ without slip and $\mathcal{G} \sim (\tau_s/\tau_0)\mathcal{B}$ with slip. (b,c) Velocity maps, normalised by the mean inlet velocity \bar{U} , at the same imposed pressure gradient, corresponding to $\mathcal{B} = 500$ in the no-slip case: (b) no slip and (c) wall slip. Wall slip lowers the bulk resistance and activates a substantially larger number of flow pathways.

to the yield limit, the model retains the correct hierarchy of active pathways and reproduces their relative velocity scales well.

We find good agreement across the full range of \mathcal{B} studied, particularly in view of the coarse-grained nature of the network description. The model reproduces the bulk response closely at small \mathcal{B} and remains quantitatively consistent as \mathcal{B} increases, although it tends to under-predict the resistance once the flow is confined to only a few active pathways. This deviation is consistent with the two main simplifications adopted here: first, the throat-scale closure is based on a reduced (one-dimensional) description of the converging-diverging gap and is least accurate for the wider constrictions that dominate transport in the strongly channelised regime; second, additional dissipation within yielded pore bodies (outside of pore-throats) is not represented explicitly. Even so, the network coupling does not amplify the local closure error, and the model retains good predictive fidelity at the macroscopic scale, with deviations of only 17% at $\mathcal{B} = 100$ and 31% at $\mathcal{B} = 10^3$. The model captures the dominant physics of yielding, channelisation, and the macroscopic departure from Darcy behaviour, providing an efficient framework for exploring these systems at a fraction of the cost of fully resolved

simulations.

We now examine the effect of wall slip on the bulk response and flow topology. Fig. 3(a) compares the dimensionless pressure gradient \mathcal{G} as a function of the bulk Bingham number \mathcal{B} for the no-slip case and for slip at the walls with $\alpha = 0.1R/K$ and $\tau_s = 0.2\tau_0$. As expected, slip reduces the resistance over the full range of \mathcal{B} , so that a lower pressure gradient is required to sustain the same bulk Bingham number. It also modifies the large- \mathcal{B} asymptote. In the no-slip limit, the strongly viscoplastic response satisfies $\mathcal{G} \sim \mathcal{B}$, whereas with slip the asymptotic scaling becomes $\mathcal{G} \sim (\tau_s/\tau_0)\mathcal{B}$. This reflects the fact that, once the bulk flow is strongly constrained, the dominant threshold is no longer set solely by bulk yielding, but also by the finite wall-slip yield stress.

The effect of slip on the flow architecture is illustrated in Fig. 3(b,c), which compares the velocity maps at the same imposed pressure gradient, corresponding to $\mathcal{B} = 500$ in the no-slip case. Without slip, the flow is confined to only two main percolating pathways. With slip, by contrast, a much larger fraction of the network remains active and several secondary paths reopen. Wall slip therefore weakens the strong channelisation observed in the no-slip case by reducing the local resistance of individual throats and allowing transport through pathways that would otherwise remain blocked. In this sense, slip alters not only the bulk pressure drop (at the same flow rate) but also the connectivity of the flowing network.

To the best of our knowledge, the inclusion of wall slip in a pore-network model for viscoplastic flow through porous media has not been reported previously, despite the fact that slip is common in yield-stress materials and can substantially modify both the threshold for motion and the distribution of flow. The present results show that incorporating slip is essential for predicting both the bulk departure from Darcy behaviour and the topology of the active flow pathways.

We now examine the near-yield behaviour of the flow. The obstacle-radius scaling of Chaparian and Tammisola¹¹, although convenient for comparison, does not collapse the $\mathcal{G} - \mathcal{B}$ curves across geometries and porosities [Fig. 4(a)]. In the plastic-dominated regime the flow is strongly channelised, with the pressure drop set primarily by dissipation in the active percolating corridors. This suggests a characteristic width h_c associated with the controlling constrictions. Near yielding, the wall stress in these corridors is $O(\tau_0)$, so

$$\frac{\Delta p}{L} \sim \frac{\tau_0}{h_c}. \quad (11)$$

Retaining the bulk groups of Chaparian and Tammisola¹¹, this suggests

$$\mathcal{G} \sim \frac{\mathcal{B}}{h_c/R}. \quad (12)$$

A recent analysis by Chaparian²⁸ proposes a porosity-based normalisation for the onset of percolation,

$$\frac{\tau_0}{R(\Delta p/L)} \sim \frac{\phi}{1-\phi}, \quad (13)$$

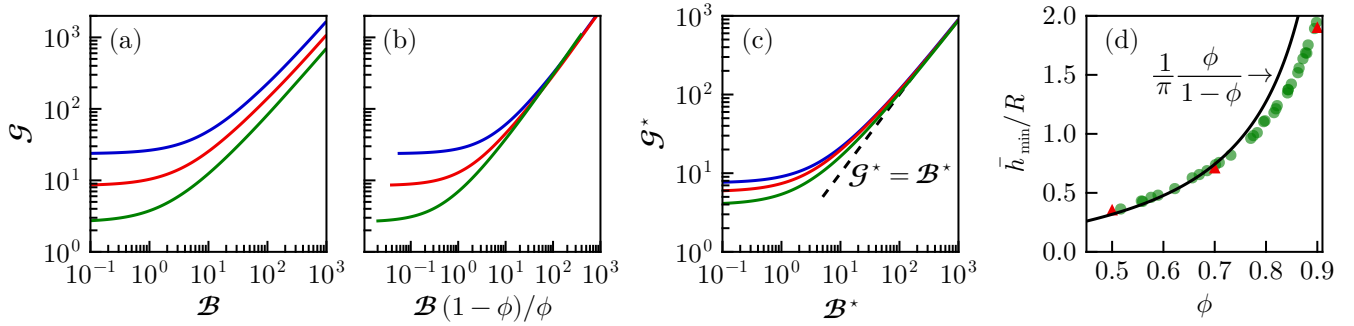


FIG. 4. Comparison of scalings for the bulk response of porous-media geometries G1 (blue), G2 (red), and G3 (green). Panels (a-c) show the dimensionless bulk pressure gradient versus bulk Bingham number using (a) the scaling of Chaparian and Tammisola¹¹, (b) the revised scaling of Chaparian²⁸, and (c) the present scaling based on \bar{h}_{\min} . (d) Dimensionless geometric length scale h_c/R versus porosity ϕ . Symbols denote random realisations of porous media (green) and the three geometries of Chaparian and Tammisola¹¹ (red). The solid black curve corresponds to the scaling of Chaparian²⁸, with prefactor $1/\pi$.

which corresponds to $h_c/R \sim \phi/(1-\phi)$ (with an empirically fitted prefactor). This substantially improves collapse [see Fig. 4(b)], but residual offsets across geometry remain.

Guided by throat-scale dissipation, we instead tie the dissipative length to a direct constriction statistics and take $h_c \sim \bar{h}_{\min}$, the domain-averaged minimum inter-obstacle half-gap. Replacing R by \bar{h}_{\min} in the definitions of new groups \mathcal{B}^* and \mathcal{G}^* gives

$$\mathcal{B}^* = \frac{\tau_0}{K(\bar{U}/\bar{h}_{\min})^n}, \quad \mathcal{G}^* = \frac{\Delta p}{L} \frac{\bar{h}_{\min}}{K(\bar{U}/\bar{h}_{\min})^n}, \quad (14)$$

for which (11) predicts the master behaviour $\mathcal{G}^* \sim \mathcal{B}^*$ in the plastic-dominated regime. Fig. 4(c) shows that, at large \mathcal{B}^* , all branches collapse onto the universal relation $\mathcal{G}^* = \mathcal{B}^*$, with negligible residual dependence on geometry. The proposed scaling therefore removes the geometry-dependent prefactor present in the original variables and identifies the dissipation-relevant length scale that governs the common linear response in the plastic-dominated regime.

Figure 4(d) shows that the measured values of \bar{h}_{\min} from multiple random realisations of porous media collapse onto a single porosity-dependent master curve across the geometries considered here. The porosity-based metric of Chaparian²⁸ follows the same overall trend, but departs from the data at high porosity, $\phi \gtrsim 0.7$. This mismatch is likely responsible for the residual offsets left by that scaling, whereas rescaling with the directly measured constriction width \bar{h}_{\min} produces the improved collapse of the bulk pressure gradient in the plastic-dominated regime shown in Fig. 4(c).

In summary, we have developed a pore-network model for Herschel-Bulkley flow in disordered porous media, including wall slip, that is specified entirely by rheological parameters and pore geometry, without fitting to flow data. Using this framework, we show that near-yield pressure losses are governed by constriction statistics rather than by an obstacle-scale length. Accordingly, rescaling with the domain-averaged minimum throat width collapses the plastic-dominated response across porosities, identifying the dissipation-relevant geometric scale that controls viscoplastic transport in this regime.

The collapse is notable because \bar{h}_{\min} is a statistical descriptor of the entire network rather than a direct measure of the final percolating pathway or a strict similarity parameter. In principle, media with the same \bar{h}_{\min} may still differ in connectivity, tortuosity, and other aspects of pore topology. Its success as a scaling length therefore suggests that, across the geometries considered here, \bar{h}_{\min} acts as an effective proxy for the constrictions statistics that control the last active pathways near yielding.

The framework also captures the leading influence of wall slip on both bulk resistance and flow topology, demonstrating that slip can substantially reduce the pressure gradient required for transport and activate pathways that remain blocked in the no-slip case. These results show that the breakdown of Darcy behaviour in yield-stress porous-media flow can be captured, and physically interpreted, within a reduced-order description.

The remaining discrepancies close to yielding are physically informative. The systematic underprediction of resistance is consistent with the fact that the dominant percolating pathway favours the widest constrictions, where the present throat-scale closure is least accurate because of its unidirectional-flow assumption. Moreover, fully resolved simulations¹¹ show additional dissipation and occasional branching within pore bodies, which are not captured when pores are represented as lossless nodes. These effects are most important precisely in the near-yield regime, where only a sparse set of pathways remains active. They therefore point to clear next refinements of the reduced-order description, rather than to a limitation of the physical picture itself. Overall, the present work provides both a predictive reduced-order tool and a physical basis for analysing yielding, channelisation, and slip in complex porous media, with broader relevance to non-Newtonian transport in disordered media.

Acknowledgements—The authors thank Qi Chen and James Shemilt for helpful discussions during model development. The authors also acknowledge support from Research IT and use of the Computational Shared Facility at The University of Manchester.

Funding—This work was supported by an EPSRC Prosper-

ity Partnership with Unilever through the Centre for Advanced Fluid Engineering and Digital Manufacturing (CAFE4DM), grant EP/R00482X/1. The authors also acknowledge support from the JSPS Overseas Challenge Program for Young Researchers, which funded an exchange placement enabling this collaboration.

- ¹R. K. Prud'homme, *Foams*, 1st ed. (CRC Press, New York, 1996).
- ²Y. Zhou, D. Yin, W. Chen, B. Liu, and X. Zhang, "A comprehensive review of emulsion and its field application for enhanced oil recovery," *Energy Science and Engineering* **7**, 1046–1058 (2019).
- ³G. H. Meeten, "Shear and compressive yield in the filtration of a bentonite suspension," *Colloids and Surfaces A: Physicochemical and Engineering Aspects* **82**, 77–83 (1994).
- ⁴T. Sochi, "Modelling the flow of yield-stress fluids in porous media," *Transport in Porous Media* **85**, 489–503 (2010).
- ⁵G. Germani, A. Stefanescu, Y. Schuurman, and A. C. van Veen, "Preparation and characterization of porous alumina-based catalyst coatings in microchannels," *Chemical Engineering Science* **62**, 5084–5091 (2007).
- ⁶T. Mori, S. Yamada, and N. Iwata, "Effects of suspension properties on the microstructure of Al_2O_3 coatings deposited onto macroporous sic substrate," *Surface and Coatings Technology* **326**, 1–10 (2017).
- ⁷R. C. G. Oliveira, J. F. Oliveira, and B. M. Moudgil, "Optimizing micro-foam rheology for soil remediation," *Progress in Colloid and Polymer Science* **128**, 298–302 (2004).
- ⁸A. R. Castro, A. B. Abdelwahed, and H. Bertin, "Saponin foam for soil remediation: On the use of polymer or solid particles to enhance foam resistance against oil," *Journal of Contaminant Hydrology* **228** (2020), 103560.
- ⁹A. R. Castro, A. B. Abdelwahed, and H. Bertin, "Enhancing pollutant removal from contaminated soils using yield stress fluids as selective blocking agents," *Journal of Contaminant Hydrology* **255** (2023), 104142.
- ¹⁰L. Talon and D. Bauer, "On the determination of a generalized Darcy equation for yield-stress fluid in porous media using a lattice-boltzmann trt scheme," *The European Physical Journal E* **36** (2013), 139.
- ¹¹E. Chaparian and O. Tammsisola, "Sliding flows of yield-stress fluids," *Journal of Fluid Mechanics* **911** (2021), a17.
- ¹²V. M. Schimmenti, F. Lanza, A. Hansen, S. Franz, A. Rosso, L. Talon, and A. De Luca, "Darcy's law of yield stress fluids on a treelike network," *Physical Review E* **108** (2023), 1023102.
- ¹³X. Zhang, E. Lorenceau, P. Basset, T. Bourouina, F. Rouyer, J. Goyon, and P. Coussot, "Wall slip of soft-jammed systems: A generic simple shear process," *Phys. Rev. Lett.* **119**, 208004 (2017).
- ¹⁴S. P. Meeker, R. T. Bonnecaze, and M. Cloitre, "Slip and flow in soft particle pastes," *Physical Review Letters* **92** (2004), 198302.
- ¹⁵J. R. Seth, M. Cloitre, and R. T. Bonnecaze, "Influence of short-range forces on wall slip in microgel pastes," *Journal of Rheology* **52** (2008), 1241.
- ¹⁶H. J. Walls, S. Brett Caines, A. M. Sanchez, and S. A. Khan, "Yield stress and wall slip phenomena in colloidal silica gels," *Journal of Rheology* **47** (2003), 847.
- ¹⁷I. Fatt, "The network model of porous media," *Transactions of the AIME* **207**, 144–181 (1956).
- ¹⁸A. Hunt and R. Ewing, *Percolation Theory for Flow in Porous Media* (Springer, Berlin Heidelberg, 2009).
- ¹⁹M. T. Balhoff and K. E. Thompson, "Modeling the steady flow of yield-stress fluids in packed beds," *AIChE Journal* **50**, 3034–3048 (2004).
- ²⁰G. G. Chase and P. Dachavijit, "Incompressible cake filtration of a yield stress fluid," *Separation Science and Technology* **38**, 745–766 (2004).
- ²¹H. C. Park, *The flow of non-Newtonian fluids through porous media*, Phd thesis, Michigan State University (1972).
- ²²T. F. Al-Fariss and K. L. Pinder, "Flow of a shear-thinning liquid with yield stress through porous media," *SPE*, 13840 (1984).
- ²³N. Waisbord, N. Stoop, D. M. Walkama, J. Dunkel, and J. S. Guasto, "Anomalous percolation flow transition of yield stress fluids in porous media," *Physical Review Fluids* **4** (2019), 063303.
- ²⁴C. Liu, A. De Luca, A. Rosso, and L. Talon, "Darcy's law for yield stress fluids," *Physical Review Letters* **122** (2019), 245502.
- ²⁵J. R. Seth, C. Locatelli-Champagne, F. Monti, R. T. Bonnecaze, and M. Cloitre, "How do soft particle glasses yield and flow near solid surfaces?" *Soft Matter* **8**, 140–148 (2012).
- ²⁶<https://www.github.com/cpfonte/yield-stress-network-model>.
- ²⁷E. Sutton, A. Juel, A. Kowalski, and C. Fonte, "Dynamics and friction losses of the flow of yield-stress fluids through 90° pipe bends," *Chemical Engineering Science* **251** (2022), 117484.
- ²⁸E. Chaparian, "Yielding to percolation: a universal scale," *Journal of Fluid Mechanics* **980**, A14 (2024).